

Magnetic ramp scale at supercritical perpendicular collisionless shocks: Full particle electromagnetic simulations

Zhongwei Yang, Quanming Lu, Xinliang Gao, Can Huang, Huigen Yang et al.

Citation: *Phys. Plasmas* **20**, 092116 (2013); doi: 10.1063/1.4821825

View online: <http://dx.doi.org/10.1063/1.4821825>

View Table of Contents: <http://pop.aip.org/resource/1/PHPAEN/v20/i9>

Published by the AIP Publishing LLC.

Additional information on Phys. Plasmas

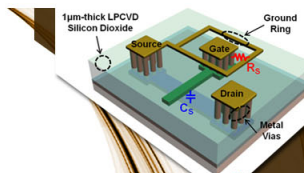
Journal Homepage: <http://pop.aip.org/>

Journal Information: http://pop.aip.org/about/about_the_journal

Top downloads: http://pop.aip.org/features/most_downloaded

Information for Authors: <http://pop.aip.org/authors>

ADVERTISEMENT



SURFACES AND INTERFACES

Focusing on physical, chemical, biological, structural, optical, magnetic and electrical properties of surfaces and interfaces, and more...

EXPLORE WHAT'S NEW IN APL

SUBMIT YOUR PAPER NOW!



ENERGY CONVERSION AND STORAGE

Focusing on all aspects of static and dynamic energy conversion, energy storage, photovoltaics, solar fuels, batteries, capacitors, thermoelectrics, and more...

Magnetic ramp scale at supercritical perpendicular collisionless shocks: Full particle electromagnetic simulations

Zhongwei Yang,^{1,2,a)} Quanming Lu,³ Xinliang Gao,³ Can Huang,³ Huigen Yang,² Ying Liu,¹ Hongqiao Hu,² and Desheng Han²

¹State Key Laboratory of Space Weather, National Space Science Center, Chinese Academy of Sciences, Beijing 100080, China

²SOA Key Laboratory for Polar Science, Polar Research Institute of China, Shanghai, 200136, China

³CAS Key Laboratory of Geospace Environment, Department of Geophysics and Planetary Science, University of Science and Technology of China, Hefei 230026, China

(Received 23 April 2013; accepted 27 August 2013; published online 23 September 2013)

Supercritical perpendicular collisionless shocks are known to exhibit foot, ramp, and overshoot structures. The shock ramp structure is in a smaller scale in contrast to other microstructures (foot and overshoot) within the shock front. One-dimensional full particle simulations of strictly perpendicular shocks over wide ranges of ion beta β_i , Alfvén Mach number M_A , and ion-to-electron mass ratio m_i/m_e are presented to investigate the impact of plasma parameters on the shock ramp scale. Main results are (1) the ramp scale can be as small as several electron inertial length. (2) The simulations suggest that in a regime below the critical ion beta value, the shock front undergoes a periodic self-reformation and the shock ramp scale is time-varying. At higher ion beta values, the shock front self-reformation is smeared. At still higher ion beta value, the motion of reflected ions is quite diffuse so that they can lead to a quasi-steady shock ramp. Throughout the above three conditions, the shock ramp thickness increases with β_i . (3) The increase (decrease) in Mach number and the decrease (increase) in the beta value have almost equivalent impact on the state (i.e., stationary or nonstationary) of the shock ramp. Both of front and ramp thicknesses are increased with M_A . © 2013 AIP Publishing LLC. [<http://dx.doi.org/10.1063/1.4821825>]

I. INTRODUCTION

Collisionless shocks are of great interest since it is commonly believed that shocks to be important sources of high-energy particles. A fraction of incident particles are reflected and accelerated within the shock transition^{1–3} where the bulk energy of plasma is converted irreversibly into thermal energy.^{4–6} Shock acceleration mechanisms are highly dependent on the shock front microstructures.⁷ Cross shock potential mainly contributed by the shock normal electric field has great impact on the particle acceleration process.^{8,9} Further study on the spatial scale of shock front microstructures will help us to understand shock acceleration mechanisms of SEPs (solar energetic particles), ACRs (anomalous cosmic rays), GCRs (galactic cosmic rays), etc.

In the last decade, shocks have obtained new interest because of the *in situ* observations by the Cluster spacecraft at Earth's bow shock. By using four spacecrafts' Cluster ion density data, Bale *et al.*¹⁰ have measured the shock transition/front scale at 98 crossings of the quasiperpendicular terrestrial bow shock. These shock profiles are fitted with a hyperbolic tangent function. They found that the convected ion gyroradius $v_{sh}/\Omega_{ci,d}$, where v_{sh} is the shock velocity in the upstream frame and $\Omega_{ci,d}$ is the ion gyrofrequency determined by the average downstream magnetic field strength, is the natural scale of the quasiperpendicular shock transition. It is in good agreement with previous studies based on the magnetic field profiles obtained by ISEE-1 and -2 at 110

quasiperpendicular bow shock crossings.¹¹ However, fitting a hyperbolic tangent to the shock would certainly not take into account the microstructures, e.g., the overshoot and also the part of the ramp leading up to it.¹²

The shock ramp structure is in a smaller scale in contrast to other microstructures (foot and overshoot) within the shock front. It plays a key role in the particle acceleration^{13,14} and thermalization.¹⁵ Both of numerical simulations^{16,17} and observations¹⁸ have clearly evidenced that the front of supercritical quasi-perpendicular shocks is nonstationary. Shock front nonstationarity can result from at least two classes of processes: one class corresponds to processes developing mainly along the shock normal. One robust process is the so called shock front self-reformation due to the accumulation of reflected ions which develops over a foot distance from the ramp.^{8,19} In brief, the self-reformation process which is usually defined as a (periodic) process where a new shock front is created in front of the old one and eventually the new one replaces the old one. The other class corresponds to processes developing along the shock front and is responsible for the shock front rippling in small^{20–22} and large scales.^{23–25} By using Cluster experimental data, Mazelle *et al.*²⁶ have shown that the ramp thickness L_r of the Earth's bow shock (e.g., in case of $\theta_{Bn} = 86 \pm 2^\circ$, $M_A = 4.1$, and $\beta_i = 0.04$, where the shock parameters θ_{Bn} , M_A , and β_i are, respectively, angle between upstream magnetic field and local shock normal, Alfvénic Mach number and ion beta value) can be comparable with a few electron inertial length $L_r \approx 5\lambda_e$ ($\lambda_e = c/\omega_{pe}$, where c is the light speed and ω_{pe} is the electron plasma frequency)²⁷ as the shock front is nonstationary. The common

^{a)}Electronic mail: zwyang@spaceweather.ac.cn.

TABLE I. Upstream plasma parameters defined for the 1-D PIC simulations (with different m_i/m_e and β_i).

Runs	1	2	3	4	5	6	7
m_i/m_e	64	100	400	1600	64	64	64
ω_{pe}/Ω_{ce}	2	2	2	2	2	2	2
β_i	0.04	0.04	0.04	0.04	0.3	0.5	1.0
β_e	0.5	0.5	0.5	0.5	0.5	0.5	0.5
V_{thi}/V_A	0.2	0.2	0.2	0.2	0.55	0.7	1.0
V_{the}/V_A	5.657	7.071	14.14	28.28	5.657	5.657	5.657
λ_i	1	1	1	1	1	1	1
λ_e	0.125	0.1	0.05	0.025	0.125	0.125	0.125
ρ_{ci}/λ_i	0.2	0.2	0.2	0.2	0.55	0.7	1.0
ρ_{ce}/λ_i	0.0884	0.0707	0.0354	0.0177	0.0884	0.0884	0.0884
M_A	4.78	4.80	4.79	4.80	4.80	4.88	4.94

method used to measure the ramp width in a shock observation is to use a linear-fitting of the magnetic field jump in the ramp.^{26,28,29} For the observationalists, further difficulties can arise from since it is very sensitive to gradients in the field profile; noise and wave activity associated with a typical bow shock observation can make localized measurements of ramp difficult. Traditional filtering does not preserve gradients well and can obscure the width of the real shock ramp. Scholer and Burgess¹² found a way to simplify the measurement of the shock ramp thickness. They investigated the shock ramp scale of quasi-stationary shocks in

high ion beta condition ($\beta_i = 1$) by fitting two straight lines to the foot and the ramp, respectively.

However, question marks remain over what kind of impact the ion-to-electron mass ratio, ion beta, and Alfvén Mach number would have on variabilities of the shock front microstructures and the ramp scale. Which physical quantity determines the shock ramp width?

In this paper, we examine the shock ramp scale at supercritical perpendicular collisionless shocks by using 1-D particle-in-cell (PIC) simulations similar to the previous works^{30,31} in order to address the above questions. In the following, we briefly describe the numerical model in Sec. II. Simulation results will be shown in Sec. III. The main conclusions are summarized in Sec. IV.

II. SIMULATION MODEL

A one-dimensional electromagnetic full particle simulation code is used to simulate the structure of a supercritical, collisionless, perpendicular shock. As in earlier work,^{12,31} shocks have high resolution in real and phase spaces. Herein, we simulate two species within our code: electrons and ions. Particles are injected on the left hand side of the simulation box with a inflow/upstream drift speed V_{inj} and are reflected at the other end. The distribution functions for the ions and electrons are Maxwellian in velocity space centered at V_{inj} . The shock is built up by the “injection method” as in

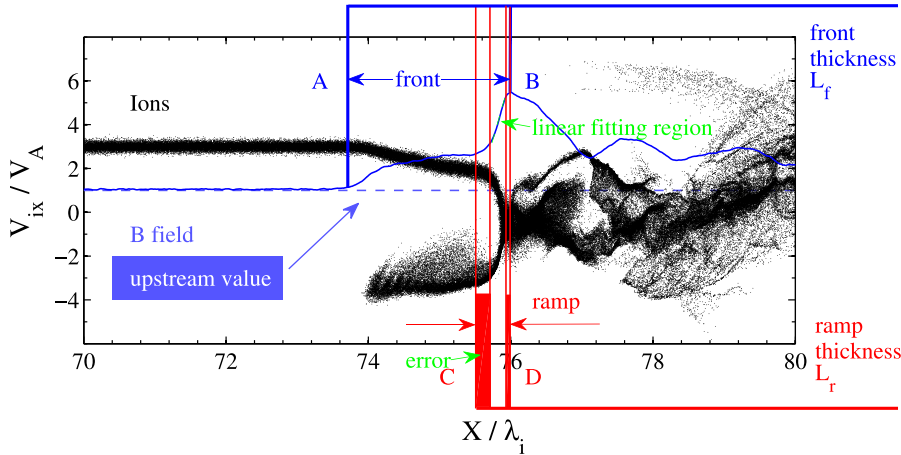


FIG. 1. Magnetic field B_y (blue) of a supercritical shock at $t = 7.2\Omega_{ci}^{-1}$ (run 1, $\beta_i = 0.04$). Ion phase space plots ($V_{ix} - X_i$) are also shown for reference (black dots). The whole shock front/transition width L_f is defined as a distance from A to B (between a pair of blue vertical lines). The shock ramp scale L_r is measured from C to D (between a pair of red vertical thick lines) and can be fitted by a straight line. Measuring error of the ramp scale is obtained through calculating the distance between pairs of red vertical thin lines about C and D.

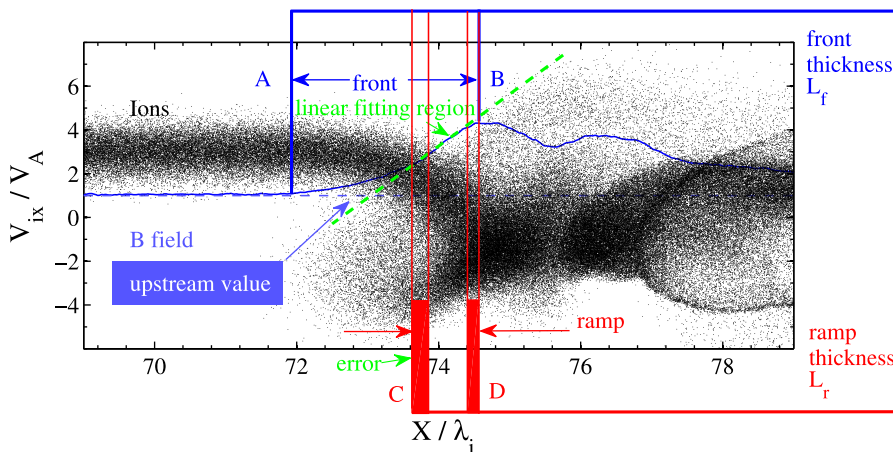


FIG. 2. Similar plots as Figure 1 for high β_i shock profile at $t = 7.2\Omega_{ci}^{-1}$ (run 7, $\beta_i = 1$).

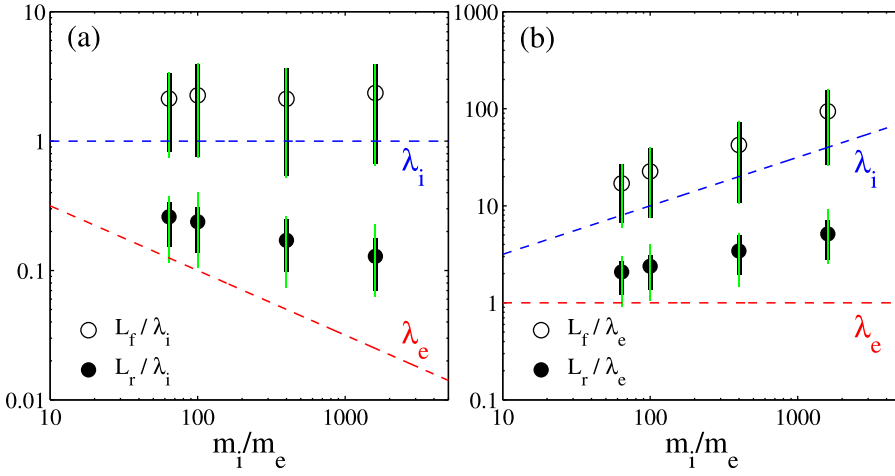


FIG. 3. The shock front thickness L_f (black circles) and the ramp thickness L_r (black dots) in units of λ_i (Panel a) and λ_e (Panel b) versus m_i/m_e . The variability of the shock ramp during the shock self-reformation and corresponding error of the measurement are marked by black and green vertical bars, respectively. The ion inertial length λ_i and electron inertial length λ_e versus m_i/m_e are also shown for reference by blue and red dashed lines.

previous works,^{32–35} and moves with a speed V_{ref} from the right-hand side toward the left. Velocities are given in units of the upstream Alfvén velocity V_A . The upstream Alfvén Mach number of the shock is $M_A = (V_{inj} + V_{ref})/V_A$ (ranges from 3.4 to 4.9). All basic parameters are as follows: plasma box size length $L_x = 90\lambda_i$, the mass ratio m_i/m_e ranges from 64 to 1600, the ion beta β_i ranges from 0.04 to 1.0 ($\beta_e = 0.5$ are kept unchanged), and the injection velocity V_{inj} ranges from $2V_A$ to $4V_A$ (corresponding to different Alfvén Mach number M_A) in different cases. The magnetic field is given in units of its upstream magnitude B_0 . Initially, there are 40 particles of each species in a grid cell. The upstream plasma is quasi-neutral.

In order to study the impact of particle dynamics on the magnetic ramp scale of a perpendicular collisionless shock, we carried out three set of runs (sets A, B, and C). Upstream

plasma parameters defined for simulations of set A are shown in Table I (runs 1–4). In set A, there are four typical runs with different values of the mass ratios m_i/m_e in order to study the impact of m_i/m_e on the ramp scale. In set B, impact of β_i on the temporal and spatial variability of the shock ramp will be investigated in detail (runs 1, 5, 6, and 7 in Table I). In set C, different cases with different injection velocities V_{inj} are carried out in order to investigate the impact of Alfvén Mach number on the ramp scale.

III. SIMULATION RESULTS

There are at least two ways to calculate the shock ramp scale. By fitting two straight lines to the foot and the ramp, Scholer and Burgess¹² defined the shock ramp scale L_r as the distance from the maximum B value in the overshoot to the

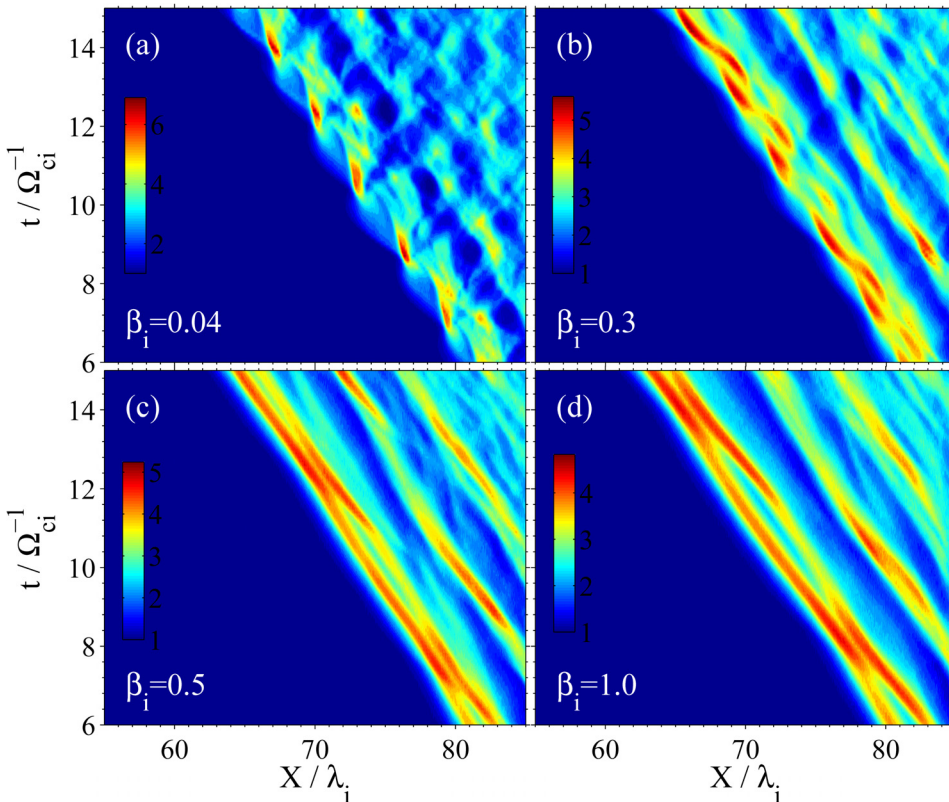


FIG. 4. The time-evolution of the perpendicular B field strength, for four simulations at various ion β_i values, over time (vertical axis, in units of Ω_{ci}^{-1}), and space (horizontal axis, in units of λ_i). All plasma parameters are identical except $\beta_i = 0.04, 0.3, 0.5,$ and 1.0 , respectively, defined for cases in panels (a), (b), (c), and (d).

intersection of the two lines. This method is succinct and effective and can be very well applied to stationary shocks. At nonstationary shocks, the shock front may suffer self-reformation and it might not be suitable for fitting by a straight line during a part of the reformation cycle. Mazelle *et al.*²⁶ fitted the shock ramp with a straight line. The start of the ramp is given by the internal limit of the exit from the foot (by eyes). An error bar is taken by defining two times, the first one when the spacecraft is likely leaving the previous microstructure (foot) and the second one when it is surely inside the next one (ramp). The end of the ramp is determined by the average downstream B value. This method can be applied to shock profiles with any arbitrary β_i . Combining with these two kinds of method, we define the ramp thickness L_r as the distance from the end of the foot (in the same way as Mazelle *et al.*²⁶) to the maximum B value in the overshoot (in the same way as Scholer and Burgess¹²). The whole shock front/transition scale L_f can be measured from the beginning point of the foot to the maximum B value in the overshoot. This combined method can be appropriate for most species of shock profiles.

We could first do a simple example to show the measurement of the shock ramp thickness. Figure 1 shows the ion phase space V_{ix} versus X_i at $t = 7.2\Omega_{ci}^{-1}$ of the run within one cyclic self-reformation of the shock front for ion $\beta_i = 0.04$ (run 1). Blue curve indicates the main magnetic field B_y of the shock. The whole shock front/transition is defined as a distance from A to B (between a pair of blue vertical lines). The shock ramp scale is measured from C to D (between a pair of red vertical thick lines) and can be fitted by a straight line as in previous works.^{12,26} Measuring error of the ramp scale is obtained through calculating the distance between pairs of red vertical thin lines at C and D. In such low β_i condition, the motion of reflected ions is very coherent and it can be described as a narrow ion ring in phase space as mentioned by Hada *et al.*⁸ At extremely high β_i (e.g., run 7), the motion of reflected ions is more diffuse. The shock foot and ramp are mixed together, and there is no clear boundary between them (see Figure 2). Both of Figures 1 and 2 show that a fraction of incident ions are reflected at the ramp region, and then these reflected ions are accumulated at the foot region. The formations of different regions (ramp

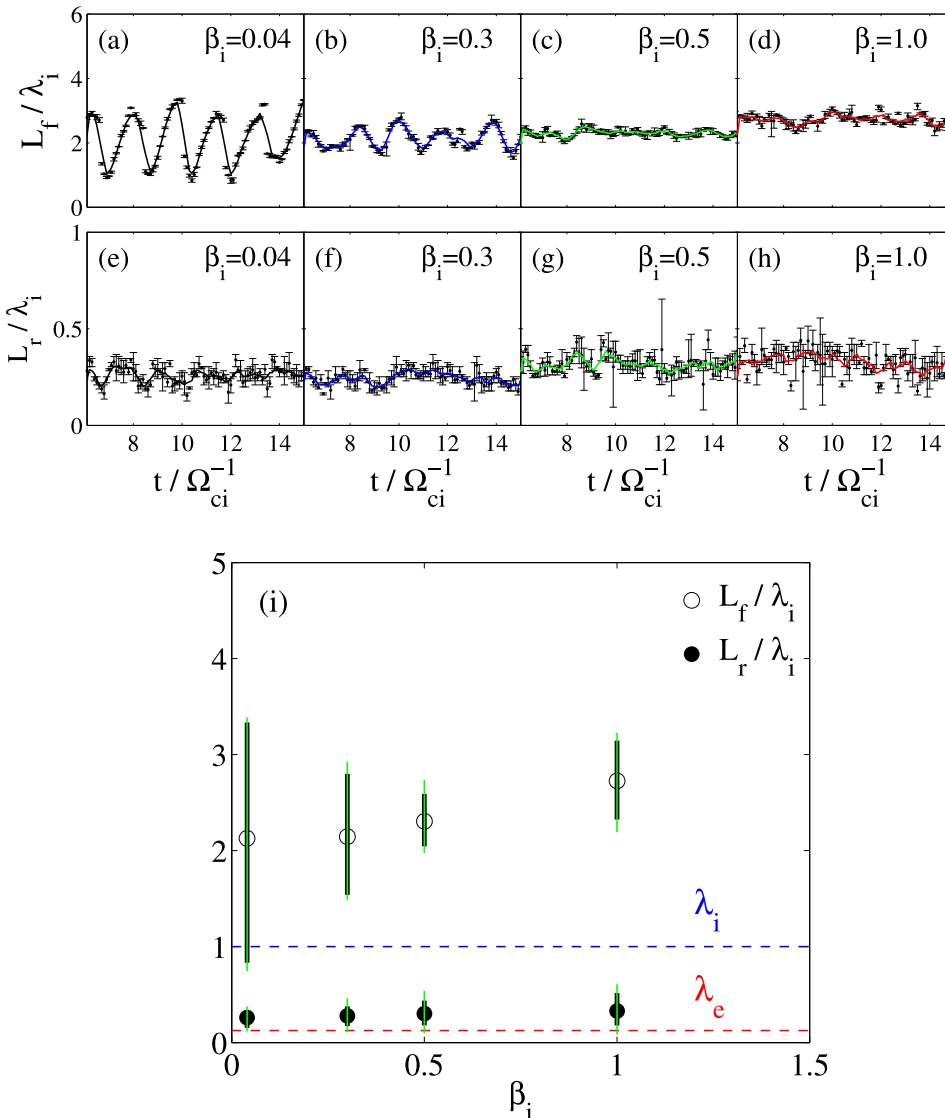


FIG. 5. Panels (a)–(d) show the variation of the shock front thicknesses L_f in unit of λ_i versus time for runs 1 ($\beta_i = 0.04$), 5 ($\beta_i = 0.3$), 6 ($\beta_i = 0.5$), and 7 ($\beta_i = 1$). Corresponding time-evolution of the shock ramp thickness L_r in unit of λ_i is shown in panels (e)–(h). Panel (i) shows the average value of L_f (black circles) and L_r (black dots) versus β_i . The variabilities of L_f and L_r at different shocks and the measuring error are marked by black and green vertical bars, respectively. The electron inertial length λ_e and the ion inertial length λ_i are also shown for reference by red and blue horizontal dotted lines.

and foot) are attributed to different statuses of particle motions (reflection and accumulation).

This paper presents the simulation results which can be separated into three parts: the impact of m_i/m_e , β_i , and M_A on the shock ramp scale will be investigated, respectively.

Firstly, we statistically study the impact of ion-to-electron mass ratio m_i/m_e on the shock ramp scale. Figs. 3(a) and 3(b) show the shock ramp thicknesses L_r (black dots) in units of λ_i and λ_e , respectively, versus m_i/m_e . The variability of the shock ramp during the shock self-reformation and the measuring error are marked by black and green vertical bars, respectively. The ion inertial length λ_i and electron inertial length λ_e versus m_i/m_e are also shown for reference by blue and red dashed lines. It is concluded that the shock ramp thickness in unit of λ_i (λ_e) is slightly decreased (increased) with the increasing m_i/m_e , and the ramp scale can be as small as several λ_e .

Secondly, we investigate the impact of ion β_i on the temporal and spatial variability of the shocks. Figure 4 shows the time-evolution of the perpendicular B field strength, for four simulations at various ion β_i values, over time (vertical axis, in units of Ω_{ci}^{-1}), and space (horizontal axis, in units of λ_i). Fig. 4(a) shows the shock in low ion beta condition ($\beta_i = 0.04$) is nonstationary. Cycles of the shock reformation are well evidenced. At middle ion beta (Fig. 4(b), $\beta_i = 0.3$), the self-reformation of the shock front becomes smeared by the diffuse reflected ions. Cycles at about $t = 8.5\Omega_{ci}$ and $t = 13.5\Omega_{ci}$ tend to blend together. This shock is in a transition stage between self-reforming and stationary shocks. At higher ion β_i (Figs. 4(c) and 4(d), $\beta_i = 0.5$ and 1.0), the shock front becomes quasi-stationary, and the self-reformation disappears because the motion of reflected ions is quite diffuse.

Figs. 5(a)–5(d) show the time-evolution of the shock front width L_f in unit of λ_i versus time for runs 1 ($\beta_i = 0.04$), 5 ($\beta_i = 0.3$), 6 ($\beta_i = 0.5$), and 7 ($\beta_i = 1$). Corresponding time-evolution of the shock ramp thickness L_r in unit of λ_i are shown in Figs. 5(e)–5(h). At lower β_i , Figs. 5(a) and 5(e) show the shock front and ramp thicknesses are varying periodically versus time because the shock is self-reforming (see Fig. 4(a)). At higher β_i , Figs. 5(c) and 5(g) show the shock front and ramp widths are gradually increased with β_i . Simultaneously, the shock front self-reformation fades out. At still higher β_i , Figs. 5(d) and 5(h) show the shock front and ramp width become larger. The bigger measuring error results from the mixing of foot and ramp at extremely large β_i case (see Figure 2). Panel (i) shows the average value of L_f (black circles) and L_r (black dots) versus β_i . The variabilities of L_f and L_r at different shocks and the measuring error are marked by black and green vertical bars, respectively. The electron inertial length λ_e and the ion inertial length λ_i are also shown for reference by red and blue horizontal dotted lines. It is concluded that both of the shock front and ramp thickness are increased with ion beta. In addition, the shock ramp scales with the electron inertial length rather than the ion inertial length no matter how much the β_i is.

Finally, we study the impact of Alfvén Mach number on the temporal and spatial variability of the shock ramp. For comparison, Figs. 6(a)–6(c) show the transition from self-reforming shocks to quasi-stationary shocks in different β_i conditions. Correspondingly, Figs. 6(d)–6(f) show the transition from self-reforming shocks to quasi-stationary shocks at different Alfvén Mach numbers (or in different injection bulk velocity V_{inj} conditions). The shock speed can be tuned by choosing the upstream injection velocity V_{inj} . A

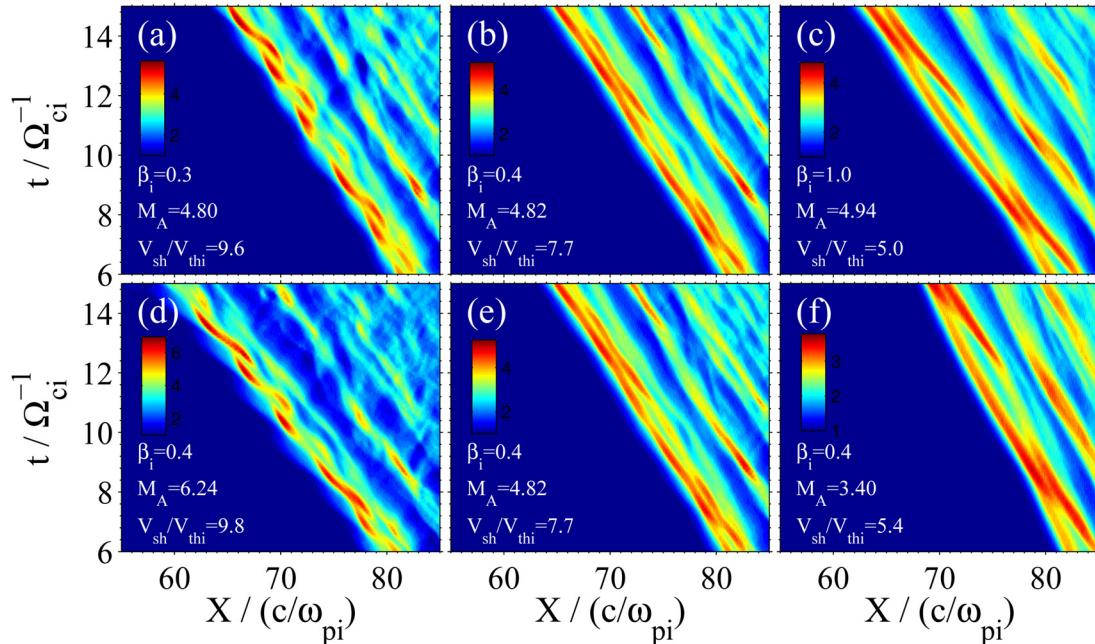


FIG. 6. Similar plots as in Figure 4. Upper panels show the shocks in different ion beta conditions: $\beta_i = 0.3$ (a), 0.4 (b), and 1 (c) ($V_{inj} = 3V_A$ is kept unchanged). From left to right, panels (a)–(c) show the transition from a self-reforming shock to a quasi-stationary shock. Lower panels show the shocks from different runs with different upstream injection bulk velocities: $V_{inj} = 4V_A$ (d), $3V_A$ (e), and $2V_A$ (f), namely, in different Alfvén Mach numbers conditions: $M_A = 6.24$ (d), 4.82 (e), and 3.4 (f) ($\beta_i = 0.4$ is kept unchanged).

TABLE II. The plasma parameters at different shocks in Figure 6.

Panels	β_i	M_A	V_{thl}/V_A	V_{sh}/V_{thi}
(a)	0.3	4.80	0.5	9.6
(b)	0.4	4.82	0.63	7.7
(c)	1.0	4.94	1.0	5.0
(d)	0.4	6.24	0.63	9.8
(e)	0.4	4.82	0.63	7.7
(f)	0.4	3.40	0.63	5.4

comparison of the plasma parameters of these shocks is listed in Table II. Table II shows a key ratio V_{sh}/V_{thi} (the impact of the M_A and β_i are taken into account together) determines the state (e.g., stationary or nonstationary) of the shock. Figs. 6(a) and 6(d) show the shock front become self-reforming in lower β_i or higher M_A condition. The shock state in the two panels is quite similar to each other because they have a similar velocity ratio ($V_{sh}/V_{thi} = 9.6$ and 9.8). Figs. 6(c) and 6(f) show the shock front becomes stationary in higher β_i or lower M_A condition. The shock state in the two panels is also quite similar to each other because they have a similar velocity ratio ($V_{sh}/V_{thi} = 5.0$ and 5.4). In summary, the increase (decrease) in Mach number and the decrease (increase) in the beta value have almost equivalent impact on the time-evolution of the shock front microstructures. Fig. 7(a) quantitatively shows both of L_f and L_r (at different shocks in Fig. 6) are increased with the Alfvén Mach number. Fig. 7(b) shows there is no clear correlation between the widths (L_f and L_r) and the ratio V_{sh}/V_{thi} . In summary, the ratio V_{sh}/V_{thi} only plays a key role in the determination of the shock front stability. The shock front becomes nonstationary and suffers self-reformation at higher ratio V_{sh}/V_{thi} .

IV. SUMMARY

In this paper, we used 1-D PIC simulations to study the impact of plasma parameters on the magnetic ramp at supercritical, perpendicular, collisionless shocks. Firstly, we examined the ion-to-electron mass ratio on the shock ramp scale. Secondly, we statistically analyze the impact of ion beta β_i on the time-evolving shock ramp scales. Finally,

impact of the ion beta and Alfvén Mach number M_A on the ramp nonstationarity are compared. The analysis has evidenced the following features:

1. We have presented 4 full particle simulations of perpendicular shocks over a ion-to-electron mass ratio regime from $m_i/m_e = 64$ to $m_i/m_e = 1600$. Both of the thicknesses of shock front and ramp in unit of the ion inertial length λ_i are decreased with the increasing mass ratio. Moreover, the ramp scale can be as small as several electron inertial length λ_e .
2. Another 4 full particle simulations of perpendicular shocks over an ion beta regime from $\beta_i = 0.04$ to $\beta_i = 1.0$ are presented. Here, the upstream injection velocity V_{inj} is fixed so that the shock speed is nearly the same. It is concluded that below the critical ion beta value ($\beta_i \sim 0.3$), the shock front undergoes a periodic self-reformation and the shock ramp scale is time-varying (e.g., $\beta_i = 0.04$). At higher ion beta values (e.g., $\beta_i = 0.3$), the shock front self-reformation is smeared. At still higher ion beta value (e.g., $\beta_i = 0.5$), the motion of reflected ions is quite diffuse so that they can lead to a quasi-steady shock ramp. Throughout the above three conditions, the shock ramp thickness increases with increasing β_i . The shock transition scale can be larger than λ_i . In contrast, the shock ramp scales with the electron inertial length λ_e no matter how much the β_i is.
3. Combining the results of the runs with different β_i and M_A , it is concluded that the increase (decrease) in Mach number and the decrease (increase) in the beta value have almost equivalent impact on the temporal and spatial variability of the shock ramp. A velocity ratio V_{sh}/V_{thi} plays a key role in the shock transition. The shock transforms from stationary shocks to self-reforming shocks when the ratio V_{sh}/V_{thi} increases. Both of shock front and ramp widths are increased with the Alfvén Mach number.

Recently, a few other plasma parameters are demonstrated to have influence on the structure of the supercritical, quasi-perpendicular shock. If a high ω_{pe}/Ω_{ce} ratio is used, a Buneman instability between reflected ions and the inflow electrons plays an important role in the foot electric field in electron inertial scale.³⁶ In their work, a very low mass ratio

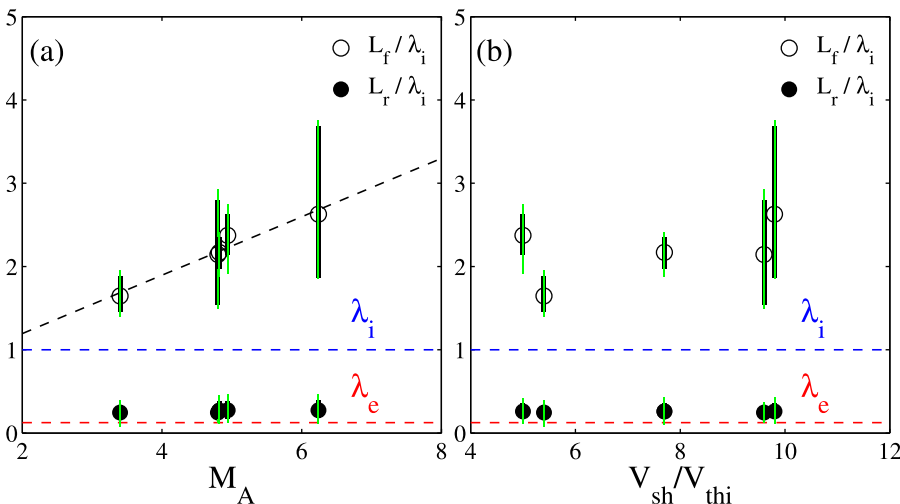


FIG. 7. The shock ramp thickness L_r (black dots) and front thickness L_f (black circles) in units of λ_i versus M_A (Panel a) and V_{sh}/V_{thi} (Panel b). The variability of the shock ramp during the shock self-reformation and corresponding error of the measurement are marked by black and green vertical bars, respectively. The ion inertial length λ_i and electron inertial length λ_e versus m_i/m_e are also shown for reference by blue and red dashed lines.

has been used in order to enable the simulations. Approaching both of the real ω_{pe}/Ω_{ce} ratio and the mass ratio m_i/m_e represents the most difficult task because of computational constraints at present time. What is the impact of particle dynamics on the shock ramp in more realistic conditions (e.g., in the solar wind at the Earth's orbit ω_{pe}/Ω_{ce} is $100\sim 200$ ³³) is our future topic. Furthermore, two-dimensional PIC simulations²¹ found that a supercritical quasi-perpendicular shock may be emitted waves, such as oblique whistler waves and lower-hybrid waves within the shock front, which may also change the structures of the shock. The ambient condition (e.g. the solar wind turbulence³⁷) and the driving source of the shocks (e.g. coronal mass ejections (CMEs) behind the CME-driven shocks^{38,39}) also need to be taken into account.

ACKNOWLEDGMENTS

The authors are grateful to B. Lembège and C. Mazelle for the helpful discussions.

This research was supported by the National Science Foundation of China under Grants No. 41204106, 41121003, 41174156, 41274148, the Specialized Research Fund for State Key Laboratories of China, the Strategic Priority Research Program on Space Science from the Chinese Academy of Sciences (XDA04060801), the CAS Key Research Program KZZD-EW-01, the Ocean Public Welfare Scientific Research Project, the State Oceanic Administration Peoples Republic of China (No. 201005017), and the Shanghai Science Foundation (12ZR1451500).

- ¹R. B. Decker and L. Vlahos, *J. Geophys. Res.* **90**, 47, doi:10.1029/JA090iA01p00047 (1985).
²Z. W. Yang, Q. M. Lu, B. Lembège, and S. Wang, *J. Geophys. Res.* **114**, A03111, doi:10.1029/2008JA013785 (2009a).
³V. D. Shapiro and D. Ucer, *Planet. Space Sci.* **51**, 665 (2003).
⁴D. A. Tidmann and N. A. Krall, *Shock Waves in Collisionless Plasmas* (Wiley, New York, 1971).
⁵B. Lembège, J. Giacalone, M. Scholer, T. Hada, M. Hoshino, V. V. Krasnoselskikh, H. Kucharek, P. Savoini, and T. Terasawa, *Space Sci. Rev.* **110**, 161 (2004).
⁶D. Burgess, E. A. Lucek, M. Scholer, S. D. Bale, M. A. Balikhin, A. Balogh, T. S. Horbury, V. V. Krasnoselskikh, H. Kucharek, B. Lembège, E. Möbius, S. J. Schwartz, M. F. Thomsen, and S. N. Walker, *Space Sci. Rev.* **118**, 205 (2005).
⁷G. P. Zank, H. L. Pauls, I. H. Carirms, and G. M. Webb, *J. Geophys. Res.* **101**, 457, doi:10.1029/95JA02860 (1996).

- ⁸T. Hada, M. Oonishi, B. Lembège, and P. Savoini, *J. Geophys. Res.* **108**, 1233, doi:10.1029/2002JA009339 (2003).
⁹Z. W. Yang, Q. M. Lu, and S. Wang, *Phys. Plasmas* **16**, 124502 (2009b).
¹⁰S. D. Bale, F. S. Mozer, and T. S. Horbury, *Phys. Rev. Lett.* **91**, 265004 (2003).
¹¹W. A. Livesey, C. F. Kennel, and C. T. Russell, *Geophys. Res. Lett.* **9**, 1037, doi:10.1029/GL009i009p01037 (1982).
¹²M. Scholer and D. Burgess, *Phys. Plasmas* **13**, 062101 (2006).
¹³M. M. Leroy, C. C. Goodrich, D. Winske, C. S. Wu, and K. Papadopoulos, *Geophys. Res. Lett.* **8**, 1269, doi:10.1029/GL008i012p01269 (1981).
¹⁴E. L. Lever, K. B. Quest, and V. D. Shapiro, *Geophys. Res. Lett.* **28**, 1367, doi:10.1029/2000GL012516 (2001).
¹⁵D. Burgess, W. P. Wilkinson, and S. J. Schwartz, *J. Geophys. Res.* **94**, 8783, doi:10.1029/JA094iA07p08783 (1989).
¹⁶D. Biskamp and H. Welter, *Nucl. Fusion* **12**, 663 (1972).
¹⁷B. Lembège and P. Savoini, *Phys. Fluids B* **4**, 3533 (1992).
¹⁸V. V. Lobzin, V. V. Krasnoselskikh, J.-M. Bosqued, J.-L. Pinçon, S. J. Schwartz, and M. Dunlop, *Geophys. Res. Lett.* **34**, L05107, doi:10.1029/2006GL029095 (2007).
¹⁹M. Scholer, I. Shinohara, and S. Matsukiyo, *J. Geophys. Res.* **108**(A1), 1014, doi:10.1029/2002JA009515 (2003).
²⁰P. Hellinger, P. Travnicek, B. Lembège, and P. Savoini, *Geophys. Res. Lett.* **34**, L14109, doi:10.1029/2007GL030239 (2007).
²¹B. Lembège, P. Savoini, P. Hellinger, and P. M. Travnicek, *J. Geophys. Res.* **114**, A03217, doi:10.1029/2008JA013618 (2009).
²²Z. W. Yang, B. Lembège, and Q. M. Lu, *J. Geophys. Res.* **117**, A07222, doi:10.1029/2011JA017211 (2012).
²³R. E. Lowe and D. Burgess, *Ann. Geophys.* **21**, 671 (2003).
²⁴F. Guo and J. Giacalone, *Astrophys. J.* **715**, 406 (2010).
²⁵F. Guo and J. Giacalone, *Astrophys. J.* **753**, 28 (2012).
²⁶C. Mazelle, B. Lembège, A. Morgenthaler, K. Meziane, T. S. Horbury, V. Genot, E. A. Lucek, and I. Dandouras, *AIP Conf. Proc.* **1216**, 471 (2010).
²⁷S. Matsukiyo, M. Scholer, and D. Burgess, *Ann. Geophys.* **25**, 283 (2007).
²⁸E. W. Greenstadt, C. T. Russell, F. L. Scarf, V. Formisano, and M. Neugebauer, *J. Geophys. Res.* **80**, 502, doi:10.1029/JA080i004p00502 (1975).
²⁹J. A. Newbury and C. T. Russell, *Geophys. Res. Lett.* **23**, 781, doi:10.1029/96GL00700 (1996).
³⁰Z. W. Yang, B. Lembège, and Q. M. Lu, *J. Geophys. Res.* **116**, A08216, doi:10.1029/2010JA016360 (2011).
³¹Q. M. Lu, Z. W. Yang, and B. Lembège, *AIP Conf. Proc.* **1500**, 241 (2012).
³²K. B. Quest, *Phys. Rev. Lett.* **54**, 1872 (1985).
³³M. Scholer and S. Matsukiyo, *Ann. Geophys.* **22**, 2345 (2004).
³⁴S. C. Chapman, R. E. Lee, and R. O. Dendy, *Space Sci. Rev.* **121**, 5 (2005).
³⁵Y. Q. Su, Q. M. Lu, X. L. Gao, C. Huang, and S. Wang, *Phys. Plasmas* **19**, 092108 (2012).
³⁶N. Shimada and M. Hoshino, *Astrophys. J.* **543**, L67 (2000).
³⁷G. Qin and A. Shalchi, *Phys. Plasmas* **20**, 092302 (2013).
³⁸Y. C.-M. Liu, M. Opher, O. Cohen, P. C. Liewer, and T. I. Gombosi, *Astrophys. J.* **680**, 757 (2008).
³⁹Y. C.-M. Liu, M. Opher, Y. Wang, T. I. Gombosi, *A&A* **527**, A46 (2011).